coatings

MDPI

Article

Effect of Heat Treatment Temperature on the Microstructure and Mechanical Properties of $Cu_{0.3}Cr_2Fe_2Ni_3Mn_2Nb_x$ High-Entropy Alloys

Fuqiang Guo [1], Chunyan Wang [1,*] and Bo Ren [2,*]

[1] Hebi Institute of Engineering and Technology, Henan Polytechnic University, Hebi 458030, China; hnxk20230181@163.com
[2] School of Mechanical Engineering, Henan University of Engineering, Zhengzhou 451191, China
* Correspondence: chen.lan00000@163.com (C.W.); renbo193513@163.com (B.R.)

Abstract: The effects of heat treatment temperature on the microstructure and mechanical properties of $Cu_{0.3}Cr_2Fe_2Ni_3Mn_2Nb_x$ high-entropy alloys (HEAs) were studied. Results indicate that in the as-cast state, an Nb_0 alloy is composed of a single FCC phase, and a Laves phase gradually forms as Nb content increases. After heat treatment at 800 °C, BCC solid solution phases rich in Cr, Fe, and Mn form in all alloys. The BCC phases in the $Nb_{0.2}$ and $Nb_{0.4}$ alloys decompose after heat treatment at 900 and 1000 °C, respectively, and the microhardness of the as-cast $Cu_{0.3}Cr_2Fe_2Ni_3Mn_2Nb_x$ HEAs increases from 127 to 203 HV with increasing Nb content. After heat treatment, the microhardness of the alloys considerably improves, and the $Nb_{0.4}$ alloy has the highest microhardness after heat treatment at 800 °C (approximately 346 HV). After heat treatment at 900 and 1000 °C, the microhardness of the three alloys decreases. The yield strength of the as-cast $Cu_{0.3}Cr_2Fe_2Ni_3Mn_2Nb_x$ HEAs increases with Nb content and shows a trend of first increasing and then decreasing with increasing heat treatment temperature. The strengthening mechanism of the heat-treated alloys is mainly attributed to the second-phase strengthening of the Laves phase and the solid solution strengthening of the BCC phase.

Keywords: high-entropy alloy; heat treatment temperature; microstructure; mechanical properties

Citation: Guo, F.; Wang, C.; Ren, B. Effect of Heat Treatment Temperature on the Microstructure and Mechanical Properties of $Cu_{0.3}Cr_2Fe_2Ni_3Mn_2Nb_x$ High-Entropy Alloys. *Coatings* **2024**, *14*, 950. https://doi.org/10.3390/coatings14080950

Academic Editor: Raul Arrabal

Received: 30 June 2024
Revised: 26 July 2024
Accepted: 28 July 2024
Published: 30 July 2024

1. Introduction

Yeh [1] and Cantor [2] first proposed the concept of high-entropy alloys (HEAs) in 2004. The so-called high-entropy alloys refer to materials composed of four or more metal elements, with an atomic percentage between 5% and 35%, and contain simple solid solution phases. Due to the mixing of multiple main elements, HEAs exhibit typical high-entropy effects, lattice distortion effects, slow diffusion effects, and cocktail effects [3]. These four typical effects result in HEAs exhibiting typical disordered FCC and BCC phases, ordered FCC and BCC phases, and HCP phases in terms of microstructure [4–12]. In addition, due to the presence of special elements (such as Ti, Nb, C, Si, and so on), HEAs often form crystal structures dominated by solid solution phases, with Laves, σ, η, R, and μ phases as secondary topological arrangement phases [13–17]. The rich and diverse crystal structure types in HEAs give them performance characteristics comparable to traditional alloys, such as high hardness, high strength, good plasticity, wear resistance, corrosion resistance, oxidation resistance, and good soft magnetic properties. Therefore, they have good application prospects in both structural and functional materials.

The $CuCr_2Fe_2Ni_2Mn_2$ alloy with a single FCC structure exhibited better corrosion resistance than traditional 304S stainless steel in both 1 M H_2SO_4 solution and 30 wt.% HNO_3 solution [18]. To further improve the corrosion resistance of the alloy, Ren et al. designed $Nb_xCu_{0.3}Cr_2Fe_2Ni_3Mn_2$ HEAs by reducing the Cu content and increasing the Ni content while introducing the corrosion-resistant Nb element. The phase structure of

the alloy changed from a single FCC phase to FCC + Laves phase, and the degree of Cu segregation was reduced. The corrosion resistance was significantly improved in 10 and 30 wt.% HNO_3 solutions [19]. However, the strength of $Cu_{0.3}Cr_2Fe_2Ni_3Mn_2$ HEA with a single FCC structure is relatively low, which limits its application. Therefore, how to improve the strength of this alloy is valuable research work. Many researchers use the method of adding solid solution strengthening elements to improve the strength of a single FCC HEA. As the Ti content increased, the FCC phase content decreased and the BCC and HCP phase content increased in the $CrFeNiNb_{0.1}Ti_x$ HEAs. The hardness of the alloy increased from 512 to 867 HV, and the yield strength of the alloy increased from 1250 to 2223 MPa [20]. As the Al content increased, the phase structure of $Al_xFeMnNiCrCu_{0.5}$ HEAs changed from dual FCC phase to dual BCC phase, and the alloy hardness increased from 216 to 518 HV [21]. Qin et al. [22] added the Nb element to CoCrCuFeNi HEA, forming FCC + Laves phase, which increased its compressive yield strength by 2.9 times. After introducing the non-metallic elements Si and C into $Fe_{2.5}CoNiCu$ HEA, the solid solution strengthening effect was increased, significantly improving the strength and hardness of the HEAs [23]. These studies indicate that introducing alloying elements with larger or smaller atomic radii into HEAs can lead to significant lattice distortion effects, resulting in stronger solid solution strengthening effects, which are beneficial for improving mechanical properties.

In addition, appropriate heat treatment of HEAs can induce phase transformation without changing the chemical composition of the alloy to improve its properties. At the same time, it can eliminate defects such as component segregation, cold cracking shrinkage, and large internal stress caused by the as-cast process. Therefore, the influence of heat treatment technology on the microstructure and properties of HEAs has become one of the current research hotspots. Sun et al. [24] conducted long-term aging of $Cr_{0.8}FeMn_{1.3}Ni_{1.3}$ HEA at 300, 500, and 700 °C and found that after aging at 500 °C for 1500 h, the alloy underwent complex phase decomposition, producing a tetragonal σ-FeCr phase, L10 NiMn phase, and a small amount of Cr-rich BCC and Fe-rich FCC phases. After aging at 700 °C for 1500 h, the alloy precipitated a Cr-rich BCC phase, forming a dual-phase microstructure, increasing the tensile strength, and decreasing ductility. The study by Yin et al. [25] on the high-temperature aging behavior of $Fe_{45}Ni_{25}Cr_{25}Mo_5$ HEA showed that the alloy exhibited a high aging hardening effect at temperatures of up to 900 °C. Moreover, owing to the precipitation of monoclinic $Cr_{5.5}Mo_{1.5}Fe_{6.5}Ni_{1.5}$ type σ phases, peak aging of 48 h was achieved at 900 °C, leading to a substantial improvement in compression performance. Chen et al. [26] found that as-cast $Al_{0.3}CrFe_{1.5}MnNi_{0.5}$ HEA was composed of BCC and FCC phases. After aging at 600 °C for 100 h, a hard intermetallic compound ρ phase ($Cr_5Fe_6Mn_8$ phase) precipitated in the alloy, achieving a high aging-hardening effect and microhardness of up to 850 HV. Ren et al.'s [27] aging study on $CuCr_2Fe_2NiMn$ alloy showed that after aging at 800 °C for 12 h, the microhardness of the alloy increased from 334 HV in the as-cast state to 450 HV. After aging at 950 and 1100 °C for 12 h, the microhardness decreased to 180 HV. The age hardening of the alloy is attributed to the precipitation of the hard intermetallic compound ρ phase from the metastable BCC phase at lower temperatures (600–800 °C), which significantly increases the hardness of the alloy. After further increasing the aging temperature to 950 °C, the ρ phase partially decomposes and completely decomposes at 1100 °C, resulting in age softening of the alloy. It can be seen that the appropriate heat treatment temperature or holding time can produce the precipitation of second phases or intermetallic compounds, and can also promote tissue refinement, thereby improving the mechanical properties of HEAs. Therefore, in this work, different contents of the Nb element were added to $Cu_{0.3}Cr_2Fe_2Mn_2Ni_3$ HEA, and $Cu_{0.3}Cr_2Fe_2Mn_2Ni_3Nb_x$ HEAs were prepared by vacuum arc furnace. Further heat treatment was performed on $Cu_{0.3}Cr_2Fe_2Mn_2Ni_3Nb_x$ HEAs at different temperatures to investigate the effect of heat treatment temperature on the microstructure and mechanical properties of the alloy system, providing experimental support and theoretical reference for the application of the alloy system in high-temperature structural materials.

2. Materials and Methods

$Cu_{0.3}Cr_2Fe_2Ni_3Mn_2Nb_x$ HEAs (x = 0, 0.2, 0.4 mol; named Nb_0, $Nb_{0.2}$, and $Nb_{0.4}$, respectively) were prepared using Cu, Cr, Fe, Ni, Mn, and Nb bulk high-purity metals (more than 99.9 wt.%). The chemical composition of the alloys is shown in Table 1. The samples were prepared via a WK-type non-consumable vacuum arc furnace. The background vacuum was 6×10^{-3} Pa during the melting process. The furnace was washed three times with high-purity argon gas, and then filled with 0.01 atm high-purity argon gas for melting protection. The chemical uniformity of the alloys was ensured by melting the alloys in a water-cooled copper mold six times. Finally, a button ingot was obtained and then processed into a sheet sample with a size of 8 mm × 6 mm × 2 mm and a compression sample with a size of 3 mm× 6 mm by wire cutting. Then, the samples were heat treated in a box-type resistance furnace at 800, 900, and 1000 °C for 12 h and cooled in the furnace. Microstructure analysis and microhardness testing were carried out after the heat-treated flake samples were ground with SiC sandpaper and polished with diamond polishing paste, and a compression performance test was carried out after the two ends of the cylindrical sample were ground flat.

Table 1. Composition of the $Cu_{0.3}Cr_2Fe_2Ni_3Mn_2Nb_x$ HEAs (mol).

Alloy	Cu	Cr	Fe	Ni	Mn	Nb
$Cu_{0.3}Cr_2Fe_2Ni_3Mn_2$ (Nb_0)	0.3	2	2	3	2	0
$Cu_{0.3}Cr_2Fe_2Ni_3Mn_2Nb_{0.2}$ ($Nb_{0.2}$)	0.3	2	2	3	2	0.2
$Cu_{0.3}Cr_2Fe_2Ni_3Mn_2Nb_{0.4}$ ($Nb_{0.4}$)	0.3	2	2	3	2	0.4

The microstructure of the HEAs after heat treatment was analyzed using X-ray diffraction (XRD, Bruker D8 ADVANCE, Bruker, Billerica, MA, USA) and scanning electron microscopy (SEM, Quanta 250, FEI Company, Hillsboro, OR, USA) systems. Cu-Kα was used for X-ray measurement at a wavelength of 1.54056 Å. The operating tube voltage and current were 40 kV and 40 mA, respectively. The scanning angle was 20°–90° (2θ), the scanning speed was 5°/min, and the scanning step was 0.02°. The composition of the HEAs was analyzed using the built-in electron spectroscopy analyzer of the SEM system. The microhardness of the HEAs was tested using an HVS-50 microhardness tester at a load of 98 N and a holding time of 20 s. Each sample was measured five times to obtain the average value as the measured hardness of the alloy. The compression performance of the HEAs was tested using an MTS810 universal testing machine at a loading rate of 2×10^{-4}/s, and three samples were measured for each alloy.

3. Results and Discussion

3.1. XRD Analysis

The XRD results of $Cu_{0.3}Cr_2Fe_2Ni_3Mn_2Nb_x$ HEAs at different heat treatment temperatures are shown in Figure 1. The Nb_0 alloy was composed of a single FCC solid solution phase in the as-cast state (Figure 1a, a1). After 800 °C heat treatment, the alloy phase structure transforms into an FCC main phase + BCC secondary phase, with a small amount of MnO. After 900 °C heat treatment, the alloy's phase structure remains an FCC main phase + BCC secondary phase. After heat treatment at 1000 °C, the phase structure of the alloy changes back to a single FCC phase, with a small amount of Fe_3O_4. The presence of MnO and Fe_3O_4 may be attributed to the incomplete removal of the oxide layer on the surface of the alloy during polishing. The $Nb_{0.2}$ alloy is composed of an FCC main phase and Laves phase as-cast (Figure 1b,b1). After 800 °C heat treatment, the alloy phase structure consists of an FCC main phase, BCC secondary phase, and a small amount of Laves phase. After 900 °C heat treatment, the BCC phase in the alloy disappears, and the phase structure is similar to the as-cast state, that is, the phase structure is FCC as the main phase and a small amount of Laves phase. After heat treatment at 1000 °C, the BCC phase forms again, and the phase structure of the alloy is transformed and forms an FCC main phase, BCC

secondary phase, and a small amount of Laves phase. The as-cast phase structure of the $Nb_{0.4}$ alloy is similar to that of the $Nb_{0.2}$ alloy (Figure 1c,c1), which are composed of FCC main and Laves phases. After heat treatment at 800 °C, some Laves phases decompose to form BCC phases, resulting in an alloy phase structure consisting of an FCC main phase, BCC secondary phase, and a small amount of Laves phase. After 900 °C heat treatment, the phase structure of the alloy is similar to that of the 800 °C heat-treated state. After heat treatment at 1000 °C, the BCC phase decomposes again, and the phase structure of the alloy transforms and forms an FCC main phase and a small amount of Laves phase.

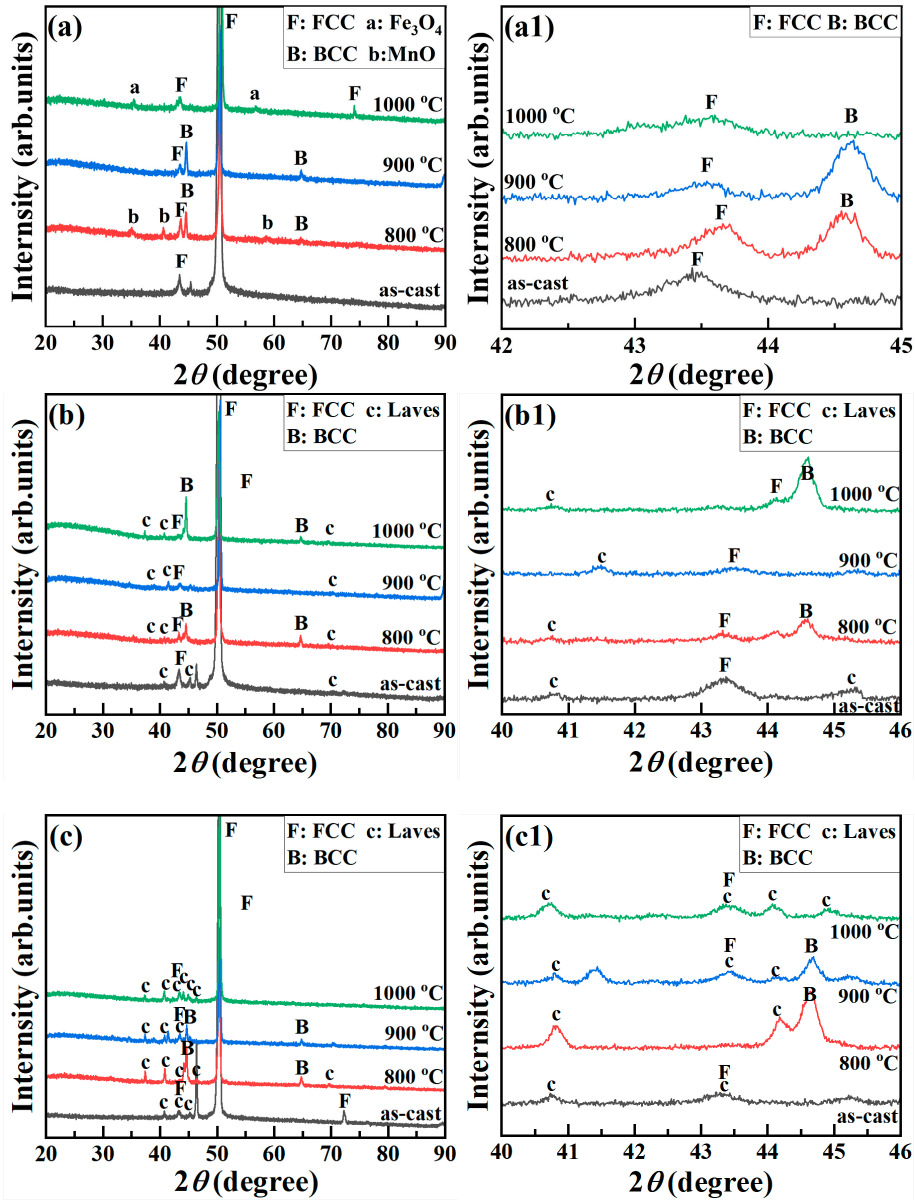

Figure 1. XRD results of $Cu_{0.3}Cr_2Fe_2Ni_3Mn_2Nb_x$ HEAs at different heat treatment temperatures: (**a**,**a1**) Nb_0; (**b**,**b1**) $Nb_{0.2}$; (**c**,**c1**) $Nb_{0.4}$.

3.2. Microstructure

Figure 2 shows the SEM images of $Cu_{0.3}Cr_2Fe_2Ni_3Mn_2Nb_x$ HEAs at different heat treatment temperatures. The microstructure of the alloys after 800 °C heat treatment exhibits dendritic and interdendritic morphology. In the map scanning results, the constituent elements of the dendritic matrix are mainly Cr, Fe, Cu, and Ni, and the constituent elements of the interdendrites are mainly Mn and Cr. After heat treatment at 900 °C, the interdendritic

morphology of the alloys disappears, and the elements are uniformly distributed, especially the short rod-shaped particles formed by the enrichment of Cr, Mn, and Fe. In addition, the Cu-Ni enrichment areas are interlaced and distributed. After heat treatment at 1000 °C, the alloys form interdendritic morphology again. The main components of the matrix are Cu and Ni, and the interdendritic morphology is divided into two zones, namely, a Cr- or Mn-rich zone and an Fe-, Cu-, or Ni-rich zone. Table 2 shows the EDS results of the microstructure of the Nb_0 HEA at different heat treatment temperatures. The XRD results in Figure 1 show that after 800 °C heat treatment, the dendritic matrix of the alloy is an FCC phase, and the interdendritic structure is a BCC phase. After 900 °C heat treatment, the short rod-shaped particles rich in Cr, Fe, and Mn constitute the BCC phase, and the matrix is the FCC phase rich in Cu, Ni, Fe, and Mn. After 1000 °C heat treatment, the interdendritic zone rich in Cr and Mn and the matrix rich in Cu, Ni, Fe, and Mn are FCC phases.

Table 2. EDS results of the microstructure of the Nb_0 HEA at different heat treatment temperatures.

Temperature	Spot	Cu	Cr	Fe	Ni	Mn
800 °C	Nominal	3.2	21.5	21.5	32.3	21.5
	1	2.7	36.0	11.2	20.2	29.9
	2	3.7	25.1	25.8	28.8	16.7
900 °C	Nominal	3.2	21.5	21.5	32.3	21.5
	1	3.3	56.6	16.3	11.2	12.5
	2	5.8	19.6	22.2	31.4	21.1
1000 °C	Nominal	3.2	21.5	21.5	32.3	21.5
	1	1.4	37.8	21.4	1.8	37.5
	2	6.6	24.1	26.8	35.3	7.3

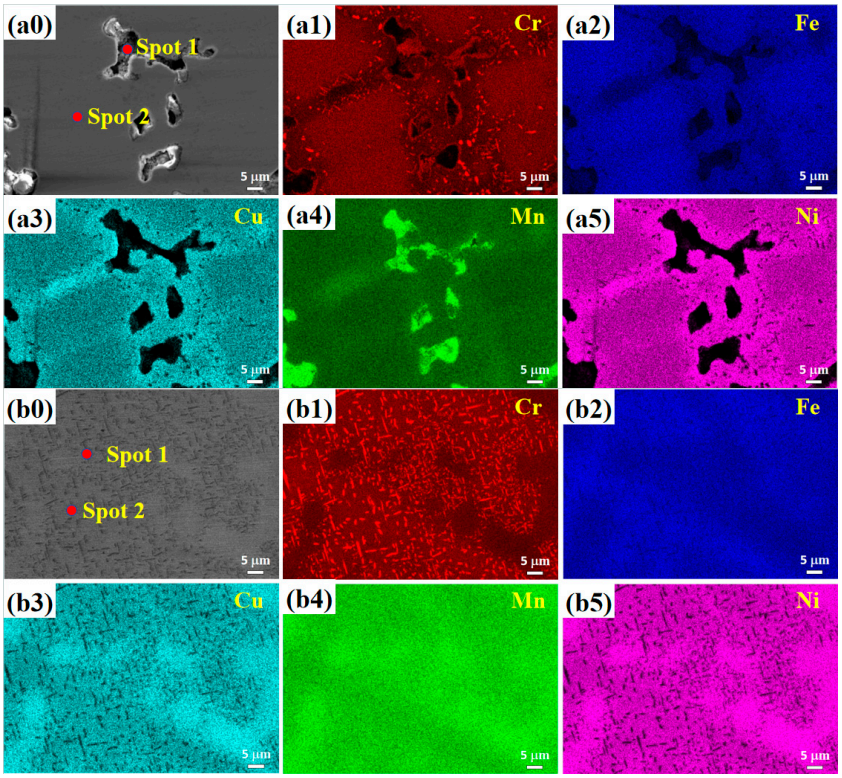

Figure 2. *Cont.*

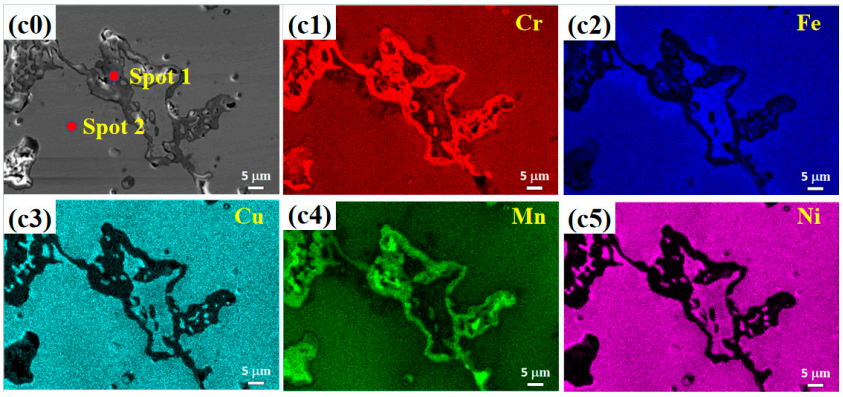

Figure 2. SEM images of the Nb_0 HEA at different heat treatment temperatures: (**a0**–**a5**) 800 °C, (**b0**–**b5**) 900 °C, (**c0**–**c5**) 1000 °C.

Figure 3 and Table 3, respectively, show SEM images and EDS results of the $Nb_{0.2}$ HEA at different heat treatment temperatures. After heat treatment at 800 °C, the dendritic matrix of the alloy is composed of Cr, Fe, Cu, Mn, and Ni, and the interdendritic structure is composed of Cu, Mn, Fe, Ni, and Nb. The EDS and XRD results show that the dendritic matrix consists of Cr-, Fe-, and Mn-rich BCC and Cu-, Mn-, Ni-, and Fe-rich FCC phases, and the interdendritic structure is also composed of Cu-, Mn-, Ni-, or Fe-rich FCC phases but includes a light-gray Nb- or Fe-rich Laves phase. After heat treatment at 900 °C, the interdendritic morphology of the alloy disappears, and microscale pit-like structures appear in the dendritic matrix, which is a Cr- and Mn-rich FCC phase. Light-gray rod-like and granular precipitates form in the matrix, which are composed of Nb-rich Laves phases. After 1000 °C heat treatment, the microstructure is similar to that formed after the 800 °C heat treatment. The BCC phase particles rich in Cr, Mn, and Fe in the matrix increase in size, and the Laves phase rich in Nb and Fe in the interdendritic region tends to aggregate.

Table 3. EDS results of the microstructure of the $Nb_{0.2}$ HEA at different heat treatment temperatures.

Temperature	Spot	Cu	Cr	Fe	Ni	Mn	Nb
800 °C	Nominal	3.2	21.1	21.1	31.6	21.1	2.1
	1	1.9	17.2	23.7	20.9	12.2	24.1
	2	7.2	16.8	19.8	32.9	22.3	0.9
900 °C	Nominal	3.2	21.1	21.1	31.6	21.1	2.1
	1	0.6	17.3	15.9	14.0	5.8	46.4
	2	6.6	22.0	22.6	33.6	14.3	0.9
1000 °C	Nominal	3.2	21.1	21.1	31.6	21.1	2.1
	1	1.8	14.7	23.3	24.1	14.5	21.5
	2	4.7	23.4	25.7	27.8	17.7	0.7

Figure 4 and Table 4, respectively, show the SEM images and EDS results of the $Nb_{0.4}$ HEA at different heat treatment temperatures. After heat treatment at 800 °C, the dendritic matrix of the alloy is composed of Cr, Fe, Cu, Mn, and Ni, and the interdendritic structure is composed of Cu, Mn, Fe, Ni, and Nb. The EDS and XRD results indicate that the dendritic matrix consists of a Cr-, Fe-, and Mn-rich BCC phase and a Cu-, Mn-, Ni-, and Fe-rich FCC phase. The interdendritic structure is a light-gray Nb- and Fe-rich Laves phase, in which the Cr-, Fe-, and Mn-rich BCC phase is dispersed in the matrix as fine particles. The Laves phase is distributed in the interdendritic region as short rods. After heat treatment at 900 °C, the BCC phase rich in Cr, Fe, and Mn is dispersed in short rod or granular form, whereas the Laves phase rich in Nb and Fe in the light-gray area is distributed in rod and granular form between dendrites. After heat treatment at 1000 °C, the matrix is composed of an FCC phase rich in Cr, Mn, Fe, Cu, and Ni, and the Laves phase rich in Nb and Fe is distributed in the matrix in the form of short rods or particles.

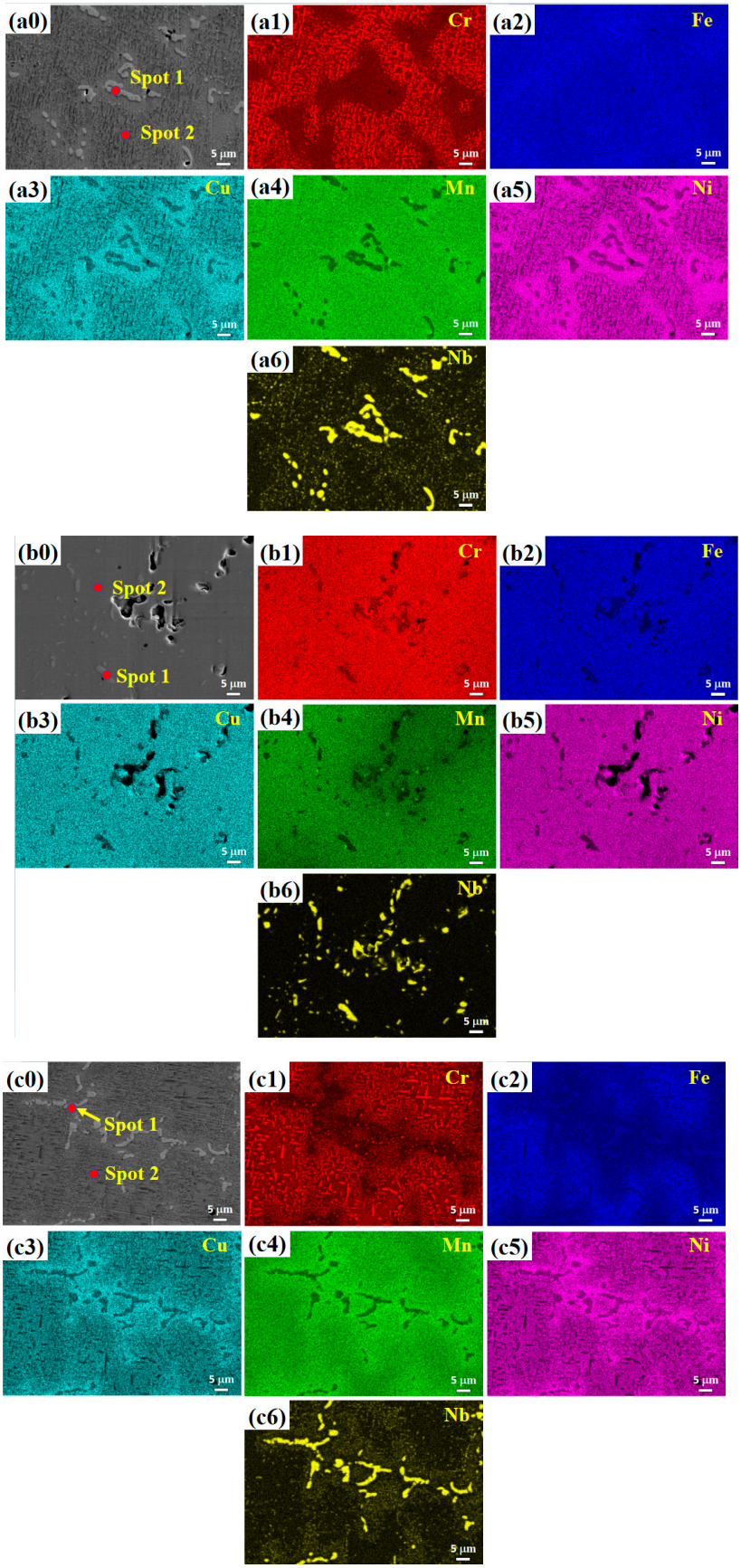

Figure 3. SEM images of the $Nb_{0.2}$ HEA at different heat treatment temperatures: (**a0**–**a6**) 800 °C, (**b0**–**b6**) 900 °C, (**c0**–**c6**) 1000 °C.

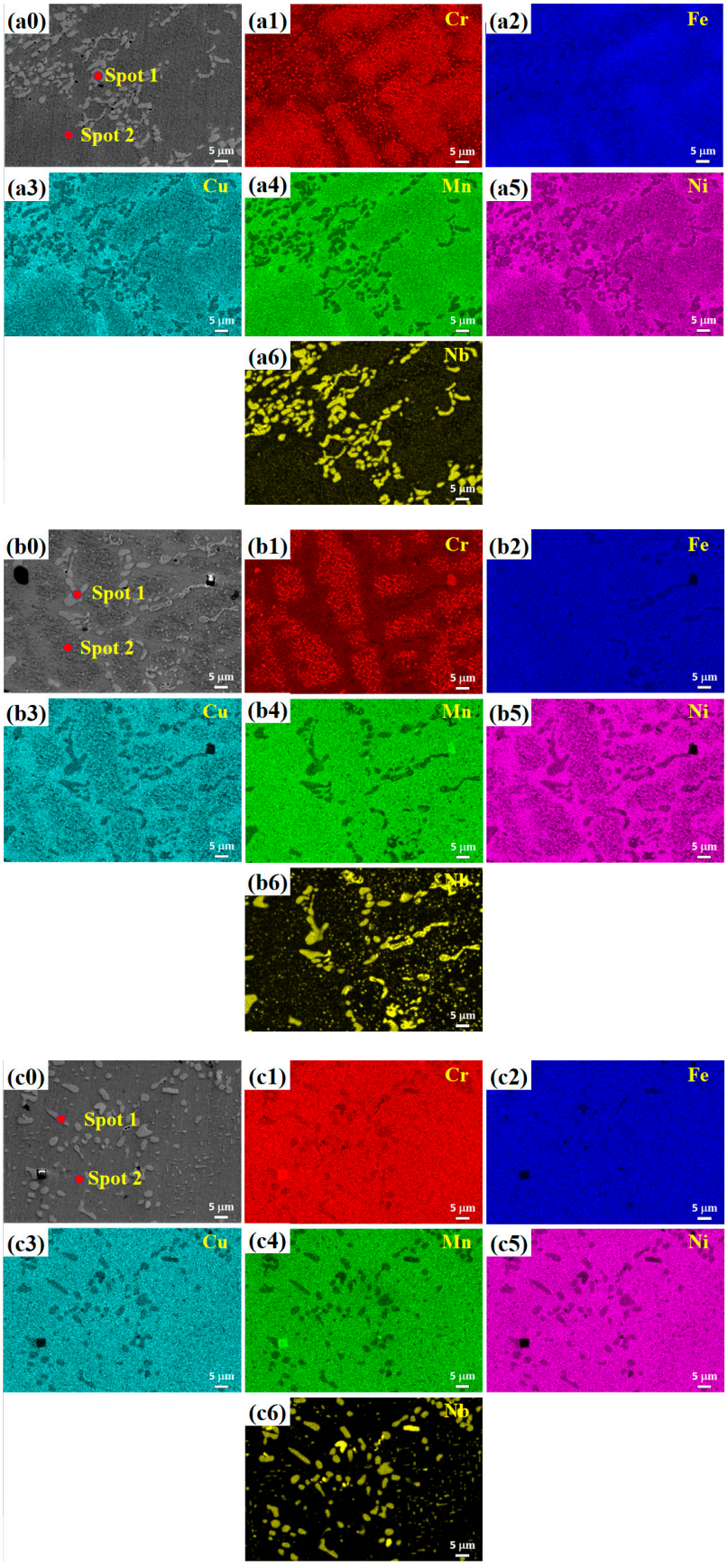

Figure 4. SEM images of the $Nb_{0.4}$ HEA at different heat treatment temperatures: (**a0**–**a6**) 800 °C, (**b0**–**b6**) 900 °C, (**c0**–**c6**) 1000 °C.

Table 4. EDS results of the microstructure of the $Nb_{0.4}$ HEA at different heat treatment temperatures.

Temperature	Spot	Cu	Cr	Fe	Ni	Mn	Nb
800 °C	Nominal	3.1	20.6	20.6	30.9	20.6	4.1
	1	1.9	14.9	24.0	23.8	13.2	22.3
	2	9.0	11.3	16.4	35.6	25.5	2.2
900 °C	Nominal	3.1	20.6	20.6	30.9	20.6	4.1
	1	1.6	17.9	23.8	21.2	11.8	23.6
	2	6.6	18.0	20.7	32.5	21.2	0.9
1000 °C	Nominal	3.1	20.6	20.6	30.9	20.6	4.1
	1	2.0	18.4	22.1	24.4	8.7	24.4
	2	6.7	20.3	20.7	33.9	17.1	1.3

In the as-cast $Cu_{0.3}Cr_2Fe_2Ni_3Mn_2Nb_x$ HEAs, as the Nb content increases, the phase structure changes from a single FCC phase to an FCC main phase with a small amount of Laves phase [19]. After heat treatment at 800–1000 °C, the phase structure, microstructure, morphology, and element distribution of the alloys undergo considerable changes. Table 5 shows the binary mixing enthalpies between the elements in the $Cu_{0.3}Cr_2Fe_2Ni_3Mn_2Nb_x$ alloy system. The binary mixing enthalpies of Cr-Fe and Cr-Mn are −1 kJ/mol and 2 kJ/mol, respectively. Under high-temperature conditions, the three elements dissolve with one another and form a BCC solid solution according to the crystal structure of Cr and Fe. The binary mixing enthalpies of Cu-Ni and Cu-Mn are both 4 kJ/mol, and Ni, Cu, and Mn are all cubic structures, which facilitates the formation of FCC phases rich in Cu, Ni, and Mn. The Ni and Mn content in this alloy system is relatively high, resulting in the formation of a phase structure dominated by the FCC solid solution. The binary mixing enthalpy of Nb-Fe is −16 kJ/mol, which is conducive to the formation of the Fe_2Nb-type Laves phase, especially at high temperatures, where more Laves phases precipitate.

Table 5. Binary mixing enthalpies between the elements in the $Cu_{0.3}Cr_2Fe_2Ni_3Mn_2Nb_x$ HEA system (KJ/mol) [28].

Element	Cr	Fe	Cu	Ni	Mn	Nb
Cr	-	−1	12	−7	2	−7
Fe		-	13	−2	0	−16
Cu			-	4	4	3
Ni				-	−8	−30
Mn					-	−4
Nb						-

3.3. Microhardness

Figure 5 shows the microhardness of $Cu_{0.3}Cr_2Fe_2Ni_3Mn_2Nb_x$ HEAs at different heat treatment temperatures. Under casting conditions, the microhardness of the Nb_0 alloy is approximately 127 HV. As the Nb content increases, the microhardness value of the alloys increases, and the microhardness of the $Nb_{0.4}$ alloy increases to 203 HV. After heat treatment at 800 °C, the microhardness of the Nb_0, $Nb_{0.2}$, and $Nb_{0.4}$ alloys increases to 190, 245, and 346 HV, respectively. After 900 °C heat treatment, the microhardness of the Nb_0 alloy remains basically unchanged at 190 HV, whereas the microhardness of the $Nb_{0.2}$ alloy increases to 280 HV, and the microhardness of the $Nb_{0.4}$ alloy decreases to 300 HV. After heat treatment at 1000 °C, the microhardness of the Nb_0 alloy decreases to 141 HV but is still higher than that of the as-cast hardness. The microhardness of the $Nb_{0.2}$ alloy considerably decreases to 122 HV, whereas the microhardness of the $Nb_{0.4}$ alloy decreases to 216 HV.

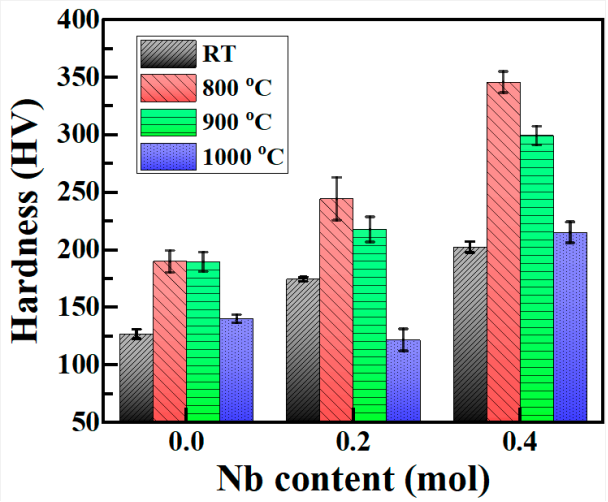

Figure 5. Microhardness of $Cu_{0.3}Cr_2Fe_2Ni_3Mn_2Nb_x$ HEAs at different heat treatment temperatures.

The as-cast hardness of the $Cu_{0.3}Cr_2Fe_2Ni_3Mn_2Nb_x$ HEAs increases with Nb content, and the increase in microhardness is mainly attributed to the precipitation strengthening of the Laves phase. The reason for the increase in microhardness of the Nb_0 alloy after heat treatment at 800 and 900 °C is attributed to the formation of the Cr-, Fe-, and Mn-rich BCC phase. Owing to the higher strength of the BCC phase compared with the FCC phase, the formation or increase in the content of the BCC phase will increase the hardness of the alloy, increasing the microhardness of the 800 and 900 °C heat-treated alloys. After heat treatment at 1000 °C, a single FCC solid solution structure forms because of the decomposition of the BCC phase in the alloys, resulting in a considerable decrease in the hardness of the alloy. However, the hardness is still higher than that in the as-cast state. The main reason for the increase in the microhardness of the $Nb_{0.2}$ alloy after 800 °C heat treatment is attributed to the formation of a Cr-, Fe-, and Mn-rich BCC phase and the precipitation of the Laves phase. The decrease in the microhardness of the alloy after 900 °C heat treatment is mainly attributed to the decomposition of the BCC phase. After heat treatment at 1000 °C, although the BCC phase forms again, the high-temperature coarsening of the BCC and Laves phases results in a decrease in alloy hardness. After heat treatment at 800 °C, the $Nb_{0.4}$ alloy precipitates the Laves phase in its microstructure, and the BCC phase is dispersed in micrometer-sized particles, which considerably improves the microhardness of the alloy. The decrease in microhardness of the alloy after 900 °C heat treatment is mainly attributed to the partial decomposition and coarsening of the BCC phase. After heat treatment at 1000 °C, the BCC phase is completely decomposed, resulting in a decrease in the hardness of the alloy.

3.4. Compression Performance

The compressive stress–strain curves of $Cu_{0.3}Cr_2Fe_2Ni_3Mn_2Nb_x$ HEAs at different heat treatment temperatures are shown in Figure 6. No fracture appears in the alloys during compression, and the compression test was stopped when a 25% strain occurred. The yield strength of these alloys is shown in Figure 7. The yield strength of the $Cu_{0.3}Cr_2Fe_2Ni_3Mn_2Nb_x$ HEAs increases with Nb content and shows a trend of first increasing and then decreasing with increasing heat treatment temperature. Under casting conditions, the yield strength of the Nb_0 alloy is approximately 192 MPa. As the Nb content increases, the yield strength of the alloys increases, and the yield strength of the $Nb_{0.4}$ alloy increases to 383 MPa. After heat treatment at 800 °C, the yield strength of the Nb_0, $Nb_{0.2}$, and $Nb_{0.4}$ alloys increased to 331, 743, and 1103 MPa, respectively. After 900 °C heat treatment, the yield strength of the Nb_0 alloy slightly increases to 344 MPa, whereas the yield strength of the $Nb_{0.2}$ and $Nb_{0.4}$ alloys decreases to 624 and 558 MPa, respectively. After heat treatment at 1000 °C, the yield strength of the Nb_0, $Nb_{0.2}$, and $Nb_{0.4}$ alloys decreases to 204, 395, and 461 MPa,

respectively, and the last two alloys have yield strengths higher than the as-cast yield strength. The mechanism underlying the improvement in the compressive yield strength of the $Cu_{0.3}Cr_2Fe_2Ni_3Mn_2Nb_x$ HEAs is the same as that underlying the enhancement of hardness and is attributed to the second-phase strengthening of the Laves phase and the solid solution strengthening of the BCC phase. The decrease in yield strength at high temperatures is mainly related to the decomposition of the BCC phase and the coarsening of the Laves phase.

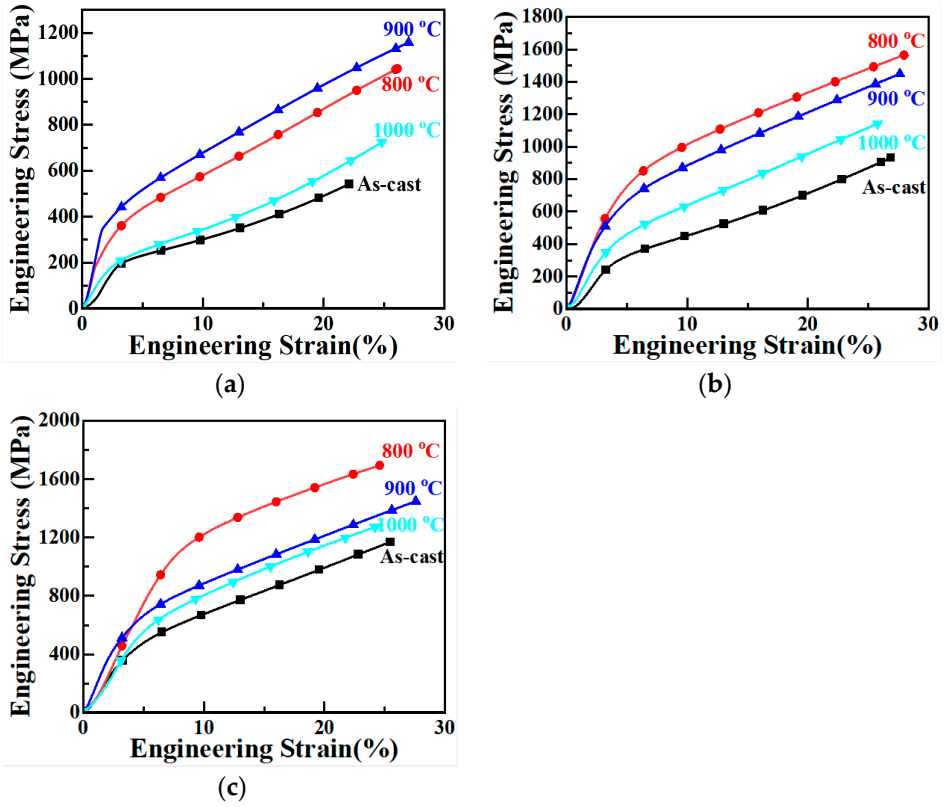

Figure 6. Compressive stress–strain curves of $Cu_{0.3}Cr_2Fe_2Ni_3Mn_2Nb_x$ HEAs at different heat treatment temperatures: (**a**) Nb_0, (**b**) $Nb_{0.2}$, (**c**) $Nb_{0.4}$.

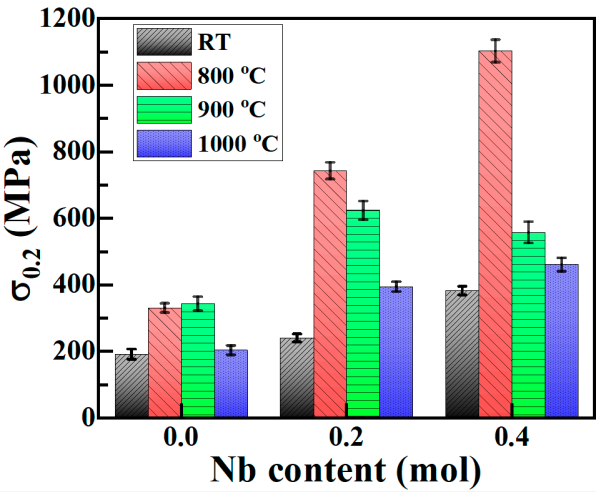

Figure 7. Yield strength of $Cu_{0.3}Cr_2Fe_2Ni_3Mn_2Nb_x$ HEAs at different heat treatment temperatures.

4. Conclusions

- (1) In the as-cast state, the Nb_0 alloy is composed of a single FCC solid solution phase. As the Nb content increases, the Laves phase gradually forms, which increases in content as the Nb content further increases. After heat treatment at 800 °C, all three alloys form BCC solid solution phases rich in Cr, Fe, and Mn. The BCC phases in the $Nb_{0.2}$ and $Nb_{0.4}$ alloys decompose after heat treatment at 900 and 1000 °C, respectively.
- (2) The microstructure of the $Cu_{0.3}Cr_2Fe_2Ni_3Mn_2Nb_x$ HEAs is basically dendritic matrix and interdendritic morphology. After heat treatment, the Laves phase is distributed in the interdendritic region in the form of rods or particles, whereas the Cr-, Fe-, and Mn-rich BCC phase and Cu-, Mn-, Ni-, and Fe-rich FCC phase are distributed in the matrix. As the heat treatment temperature increases, the Laves phase aggregates and grows, whereas the BCC phase coarsens or decomposes.
- (3) As the Nb content increases, the microhardness of the as-cast $Cu_{0.3}Cr_2Fe_2Ni_3Mn_2Nb_x$ HEAs increases from 127 to 203 HV. After heat treatment, the microhardness of the alloys substantially improves, with the $Nb_{0.4}$ alloy having the highest microhardness after 800 °C heat treatment, approximately 346 HV. After heat treatment at 900 and 1000 °C, the microhardness of the three alloys decreases. The increase in Nb content in the as-cast hardness is mainly attributed to the precipitation strengthening of the Laves phase. After heat treatment, the hardness of the alloys first increases and then decreases mainly due to the formation and decomposition of the BCC phase and the coarsening of the Laves phase.
- (4) The yield strength of the as-cast $Cu_{0.3}Cr_2Fe_2Ni_3Mn_2Nb_x$ HEAs increases with Nb content and first increases and then decreases with increasing heat treatment temperature. When cast, the yield strength of the $Nb_{0.4}$ alloy is the highest (approximately 383 MPa). After heat treatment at 800 °C, its yield strength increases to 1103 MPa. The mechanism underlying the improvement in the compressive yield strength of these alloys is the same as the hardness-enhancing mechanism owing to the second-phase strengthening of the Laves phase and the solid solution strengthening of the BCC phase.

Author Contributions: Methodology, B.R. and C.W.; investigation, F.G. and B.R.; resources, C.W.; data curation, F.G.; writing—original draft preparation, B.R.; writing—review and editing, B.R. and F.G.; project administration, B.R. and F.G.; funding acquisition, B.R. All authors have read and agreed to the published version of the manuscript.

Funding: This research was funded by the Henan Province Science and Technology Research Plan Project, Grant No. 232102231007.

Institutional Review Board Statement: Not applicable.

Informed Consent Statement: Informed consent was obtained from all subjects involved in the study.

Data Availability Statement: All the raw/processed data required to reproduce these findings are available and can be requested from the authors.

Conflicts of Interest: The authors declare no conflicts of interest.

References

1. Yeh, J.W.; Chen, S.K.; Lin, S.J.; Can, J.Y.; Chin, T.S.; Shun, T.T. Nanostructured high entropy alloys with multiple principal elements: Novel alloy design concepts and outcomes. *Adv. Eng. Mater.* **2004**, *6*, 299–303. [CrossRef]
2. Cantor, B.; Chang, I.T.H.; Knight, P.; Vincent, A.J.B. Microstructure development in equiatomic multicomponent alloys. *Mater. Sci. Eng. A* **2004**, *375–377*, 213–218. [CrossRef]
3. Zhang, Y.; Zuo, T.T.; Tang, Z.; Gao, M.C.; Dahmen, K.A.; Liaw, P.K.; Lu, Z.P. Microstructures and properties of high-entropy alloys. *Prog. Mater. Sci.* **2014**, *61*, 1–93. [CrossRef]
4. Pang, J.Y.; Xiong, T.; Yang, W.F.; Ge, H.L.; Zheng, X.D.; Song, M.; Zhang, H.W.; Zheng, S.J. Atomic scale structure dominated FCC and B2 responses to He ion irradiation in eutectic high-entropy alloy $AlCoCrFeNi_{2.1}$. *J. Mater. Sci. Technol.* **2022**, *129*, 87–95. [CrossRef]

5. Tripathy, B.; Saha, R.; Bhattacharjee, P.P. Microstructure and unusually strong recrystallization texture of the FCC phase of a cost-effective high-strength dual-phase $AlCrFe_2Ni_2$ high entropy alloy. *Intermetallics* **2022**, *145*, 107559. [CrossRef]
6. Shun, T.T.; Hung, C.H.; Lee, C.F. Formation of ordered/disordered nanoparticles in FCC high entropy alloys. *J. Alloys Compd.* **2010**, *493*, 105–109. [CrossRef]
7. Qiao, D.X.; Liang, H.; Wu, S.Y.; He, J.Y.; Cao, Z.Q.; Lu, Y.P.; Li, T.J. The mechanical and oxidation properties of novel B2-ordered $Ti_2ZrHf_{0.5}VNb_{0.5}Al_x$ refractory high-entropy alloys. *Mater. Charact.* **2021**, *178*, 111287. [CrossRef]
8. Jin, D.M.; Wang, Z.H.; Yuan, J.H.; Jiang, B.B.; Yu, F.Y.; Li, J.F.; Wang, Q. High-strength and energetic $Al_2Ti_6Zr_2Nb_3Ta_3$ high entropy alloy containing a cuboidal BCC/B2 coherent microstructure. *J. Alloys Compd.* **2023**, *931*, 167546. [CrossRef]
9. Wang, L.; Wang, J.R.; Niu, H.W.; Yang, G.J.; Yang, L.; Xu, M.Q.; Yi, J.J. BCC+L21 dual-phase $Cu_{40}Al_{20}Ti_{20}V_{20}$ near-eutectic high-entropy alloy with a combination of strength and plasticity. *J. Alloys Compd.* **2022**, *908*, 164683. [CrossRef]
10. Yurchenko, N.Y.; Panina, E.S.; Zherebtsov, S.V.; Tikhonovsky, M.A.; Salishchev, G.A.; Stepanov, N.D. Microstructure evolution of a novel low-density Ti-Cr-Nb-V refractory high entropy alloy during cold rolling and subsequent annealing. *Mater. Charact.* **2019**, *158*, 109980. [CrossRef]
11. Takeuchi, A.; Amiya, K.; Wada, T. High-entropy alloys with a hexagonal close-packed structure designed by equi-atomic alloy strategy and binary phase diagrams. *JOM* **2014**, *66*, 1984–1992. [CrossRef]
12. Lužnik, J.; Koželj, P.; Vrtnik, S.; Jelen, A.; Jagličić, Z.; Meden, A.; Feuerbacher, M.; Dolinšek, J. Complex magnetism of Ho-Dy-Y-Gd-Tb hexagonal high-entropy alloy. *Phys. Rev. B* **2015**, *92*, 22420122. [CrossRef]
13. Ren, H.; Chen, R.R.; Gao, X.F.; Liu, T.; Qin, G.; Wu, S.P.; Guo, J.J. Phase formation and mechanical features in $(AlCoCrFeNi)_{100-x}Hf_x$ high-entropy alloys: The role of Hf. *Mater. Sci. Eng. A* **2022**, *858*, 144156. [CrossRef]
14. Zhi, Q.; Tan, X.R.; Xie, J.L.; Liu, Y.; Yang, K.; Zhang, Q.; Liu, W.H.; Liu, Z.X. Microstructure and properties of lightweight $Al_2NbTi_xV_2Zr$ high entropy alloy. *J. Mater. Eng. Perform.* **2022**, *31*, 4934–4944. [CrossRef]
15. Dong, Y.; Lu, Y.P.; Jiang, L.; Wang, T.M.; Li, T.J. Effects of electro-negativity on the stability of topologically close-packed phase in high entropy alloys. *Intermetallics* **2014**, *52*, 105–109. [CrossRef]
16. Huang, Y.B.; Hu, Y.L.; Zhang, M.J.; Mao, C.; Tong, Y.G.; Zhang, J.; Li, K.W.; Wang, K.M. On the enhanced wear resistance of laser-clad $CoCrCuFeNiTi_x$ high-entropy alloy coatings at elevated temperature. *Tribol. Int.* **2022**, *174*, 107767. [CrossRef]
17. Liang, H.; Hou, J.X.; Jiang, L.; Cao, Z.Q. Microstructure and dry-sliding wear resistance of CoCrFeNiMoTix high entropy alloy coatings produced by laser cladding. *Coatings* **2024**, *14*, 221. [CrossRef]
18. Ren, B.; Liu, Z.X.; Li, D.M.; Shi, L.; Cai, B.; Wang, M.X. Corrosion behavior of CuCrFeNiMn high entropy alloy system in 1M sulfuric acid solution. *Mater. Corros.* **2012**, *63*, 828–834. [CrossRef]
19. Ren, B.; Liang, Y.C.; Zhang, X.F.; Yu, Y.; Zhao, R.F.; Jiang, A.Y.; Liu, J.X.; Zhou, Y.J.; Zhang, B.F.; Liu, Z.X. Corrosion behavior of $Nb_xCu_{0.3}Cr_2Fe_2Ni_3Mn_2$ high-entropy alloys in HNO_3 solution. *Results Phys.* **2023**, *51*, 106780. [CrossRef]
20. Zhang, M.D.; Zhang, L.J.; Fan, J.T.; Yu, P.F.; Li, G. Novel Co-free $CrFeNiNb_{0.1}Ti_x$ high-entropy alloys with ultra high hardness and strength. *Mater. Sci. Eng. A* **2019**, *764*, 138212. [CrossRef]
21. Nguyen, T.; Huang, M.; Li, H.J.; Hong, L.; Yang, S. Effect of Al content on microstructure and mechanical properties of as-cast $Al_xFeMnNiCrCu_{0.5}$ high-entropy alloys. *Mater. Sci. Eng. A* **2022**, *832*, 142495. [CrossRef]
22. Qin, G.; Wang, S.; Chen, R.R.; Gong, X.; Wang, L.; Su, Y.Q.; Guo, J.J.; Fu, H.Z. Microstructures and mechanical properties of Nb-alloyed CoCrCuFeNi high-entropy alloys. *J. Mater. Sci. Technol.* **2018**, *34*, 365–369. [CrossRef]
23. Wu, J.; Qiu, H.; Zhu, H.G.; Xie, Z.H.; Cheng, J.L. Influences of Si and C addition on microstructure and mechanical properties of $Fe_{2.5}CoNiCu$ high-entropy alloy. *Trans. Nonferrous Met. Soc. China* **2023**, *33*, 3406–3417. [CrossRef]
24. Sun, H.T.; Liu, T.; Oka, H.; Hashimoto, N.; Cao, Y.; Luo, R. Role of aging temperature on thermal stability of Co-free $Cr_{0.8}FeMn_{1.3}Ni_{1.3}$ high-entropy alloy: Decomposition and embrittlement at intermediate temperatures. *Mater. Charact.* **2024**, *210*, 113804. [CrossRef]
25. Yin, Y.; Chen, Z.H.; Mo, N.; Kent, D.; Candella, A.R.; Koey, K.E.; Tan, Q.; Bermingham, M.; Zhang, M.X. High-temperature age-hardening of a novel cost-effective $Fe_{45}Ni_{25}Cr_{25}Mo_5$ high entropy alloy. *Mater. Sci. Eng. A* **2020**, *788*, 139580. [CrossRef]
26. Chen, S.T.; Tang, W.Y.; Kuo, Y.F.; Chen, S.Y.; Tsau, C.H.; Shun, T.T.; Yeh, J.W. Microstructure and properties of age-hardenable $Al_xCrFe_{1.5}MnNi_{0.5}$ alloys. *Mater. Sci. Eng. A* **2010**, *527*, 5818–5825. [CrossRef]
27. Ren, B.; Liu, Z.X.; Cai, B.; Wang, M.X.; Shi, L. Aging behavior of a $CuCr_2Fe_2NiMn$ high-entropy alloy. *Mater. Des.* **2012**, *33*, 121–126. [CrossRef]
28. Takeuchi, A.; Inoue, A. Classification of bulk metallic glasses by atomic size difference, heat of mixing and period of constituent elements and its application to characterization of the main alloying element. *Mater. Trans.* **2005**, *46*, 2817–2829. [CrossRef]